Yang, Q., Dai, Q., Han, D., Chen, Y., & Zhang, S. (2019). Sensitivity analysis of raindrop size distribution parameterizations in WRF rainfall simulation. *Atmospheric Research*, *228*, 1-13. https://doi.org/10.1016/j.atmosres.2019.05.019

Sensitivity analysis of raindrop size distribution parameterizations in WRF rainfall simulation

Qiqi Yang [1,2,3], Qiang Dai [1,2,3,*], Dawei Han [2], Yiheng Chen [2] and Shuliang Zhang [1,3]

[1]Key Laboratory of VGE of Ministry of Education, Nanjing Normal University, Nanjing, China
[2]WEMRC, Department of Civil Engineering, University of Bristol, Bristol, UK
[3]Jiangsu Center for Collaborative Innovation in Geographical Information Resource Development and Application, Nanjing, China
[*]Correspondence: q.dai@njnu.edu.cn or dqgis@hotmail.com

Abstract:

Numerical weather models such as WRF (Weather Research and Forecasting) are increasingly used in studies on water resources. However, they have suffered from relatively poor performance in rainfall estimation. Among the various influential factors, a critical parameter in the WRF model rainfall retrieval is raindrop size distribution (DSD), which has not been fully explored. The analysis of sensitivity and uncertainty of the DSD model accuracy is significant for rainfall forecasts based on mesoscale numerical weather prediction (NWP) models. A WRF-disdrometer integrated error assessment framework is developed to analyze the accuracy and sensitivity of DSD parameterizations of gamma distribution in WRF rainfall simulation. This study adopts three different microphysics parameterizations (Morrison, WDM6, and Thompson aerosol-aware) to simulate the DSD of approximately one hundred rainfall events in Chilbolton, UK that are categorized into 12 scenarios based on the season, rainfall evenness, and rainfall rate. The Thompson aerosol-aware microphysics scheme shows the best performance among the three. In comparisons of WRF rainfall simulations across different scenarios of evenness and rainfall rate, a higher accuracy is obtained with more even rain and a higher rainfall rate. The sensitivity results of different DSD parameterizations indicate that the sensitivity to the intercept parameter N_0 is pronouncedly higher than those to the shape parameter μ and slope parameter λ for all studied schemes. The overall WRF rainfall shows a trend of slight underestimation followed by overestimation as μ increases; further, the rainfall is overestimated when $log_{10}N_0$ or λ decreases and is underestimated when it increases and then remains constant. Comparisons of different scenarios reveal that variations of DSD parameters of even rain have a relatively high impact on rainfall recognizability, and the DSD parameterizations show a higher sensitivity for rainfall with a low rate. Moreover, the sensitivity discrimination is not clear among the rainfall of different seasons. The uncertainty assessment of the WRF rainfall retrieval caused by the shape parameter suggests that a gamma DSD model with a variable shape parameter should be developed according to the evenness, rainfall rate, and microphysics parameterizations by using the WRF model. Some modified algorithms of the WRF gamma DSD model for achieving better accuracy in WRF rainfall retrievals will be explored in future studies with various climatic regimes by adjusting the DSD

parameterization based on the assimilation of measured data.

Keywords: Raindrop size distribution, WRF, rainfall simulation, microphysics parameterization, Morrison, WDM6, Thompson aerosol-aware, disdrometer

1. Introduction

The raindrop size distribution (DSD) spectrum, which is an integral product of hydrometeor size distribution where the drop size ranges from that of drizzle rain to that of hailstone (Iguchi et al., 2012), is frequently modeled by an analytical function such as the exponential function, gamma function, and lognormal distribution (Bringi et al., 2002; K'ufre-Mfon et al., 2015). The DSD model depends on several precipitation microphysics processes, such as evaporation, condensation and deposition, collision, raindrop breakup, and freezing (Tapiador et al., 2010). Accordingly, the characteristics of DSD spectra are important to the accuracy of precipitation and rainfall retrieval and for understanding the processes involved in precipitation variation, cloud microphysics, radar remote sensing, and radio communications (Kirankumar et al., 2008). Additionally, the raindrop size is required to calculate rainfall kinetic energy, which is a significant factor in the estimation of soil erosion (Angulo-Martínez et al., 2016; Meshesha et al., 2016).

DSD can be obtained using instruments such as a ground disdrometer, weather radar, and satellite or by using numerical forecast models such as the mesoscale numerical weather prediction (NWP) system. For data-scarcity areas without rainfall gauges or weather radars, the NWP model is a valuable tool for precipitation forecasting or simulation. In addition, it can be used to study the details of sophisticated microphysical cloud processes that cannot be directly observed by measurement platforms with a high resolution; thus, it can further assist and substantiate discoveries from observational studies (Jung et al., 2010). The weather research and forecasting (WRF) model is the latest-generation mesoscale NWP system that is used as utility-downscaling software for many research fields including atmospheric research, weather prediction, climate change, and hydrology. The WRF model provides numerous options of cloud microphysical schemes with different DSD models and parameterizations (Han et al., 2013). However, it is necessary to evaluate the WRF DSD retrieval algorithm with appropriate observations to evaluate the fidelity of the simulated structure (Brown et al., 2016). The disdrometer, a ground-based instrument, can automatically take the measurements of particle drop sizes and provide precise information on the DSD, rainfall rate, and reflectivity factor (Bringi et al., 2003; Islam et al., 2012). It can efficiently capture the microphysics structure of precipitation; thus, it is useful for the validation of the WRF model.

The raindrop size distribution and DSD model parameters in the WRF model are mainly determined by the microphysics parameterization setting. The spectral bin and bulk microphysics parameterization schemes are the two main approaches to model the cloud and precipitation microphysics processes (Milbrandt and Yau, 2005). Compared to the spectral bin approach, bulk microphysics parameterizations are simple and computationally efficient; thus, they are adopted broadly in the WRF model (Johnson et al., 2016; Kogan and Belochitski, 2012). The bulk microphysics schemes commonly assume the DSD model as a gamma distribution with an intercept, a slope, and shape parameters, and these schemes can be classified into single-, double-, and triple-moment schemes based on physical quantities such as the mass mixing ratio, total number

concentration, and radar reflectivity factor (Johnson et al., 2016). The intercept parameter, N_0, in most single-moment schemes is constant for a given precipitation species because the number concentration of species is not predicted (Morrison et al., 2009; Dudhia 1989; Lin et al., 1983), while N_0 evolves freely in double- and triple-moment schemes, which enables a greater flexibility of drop-size distribution. Consequently, double- and triple-moment schemes yield more complicated and superior microphysical processes, resulting in better performance in the supercell storm and convection-scale simulation than single-moment schemes (Lim and Hong, 2010; Morrison et al., 2009; Morrison and Pinto, 2005). Although triple-moment schemes can also predict the radar reflectivity factor, several studies concluded that double- and triple-moment simulations are qualitatively similar in many terms; however, triple-moment schemes have an increased computational expense (Dawson et al., 2010; Milbrandt and Yau, 2006). As a result, some bulk microphysics schemes fix the shape parameter in the gamma DSD model without considering the uncertainty associated with the DSD parameterizations, which is important in evaluating the overall performance of WRF rainfall retrieval algorithms.

Many recent studies have highlighted the sensitivity of WRF forecasts to the choice of microphysics by simulating several typical rainfall events such as tropical cyclones and convective storms (Brown et al., 2016; Kala et al., 2015; Khain et al., 2016; Shrestha et al., 2017). For instance, Brown et al. (2016) investigated the WRF capture performance of two hurricanes by using six different microphysics schemes. In addition, some other studies stated that the adopted DSD model of microphysics schemes are significantly sensitive to the particle sizes in the inherent atmospheric course (Ćurić et al., 2010; Ćurić et al., 2009; Gilmore et al., 2004). For example, Gilmore et al. (2004) illustrated the impact of different raindrop size distributions on the variation in rainfall accumulations and showed great ambiguities in the modelled outputs. Thus, the DSD model, which depends on the choice of microphysics schemes and particle parametric variables, is extremely important for the accuracy and uncertainty of WRF rainfall retrieval. However, few studies in the literature have focused on the sensitivity related to the DSD parameterizations, which directly determine the raindrop size distribution, rainfall rate, radar reflectivity factor, and so on. On the other hand, considering the large uncertainty of WRF rainfall simulation, research efforts are being increasingly paid to correcting weather forecasts with meteorological observations via data assimilation. We believe that data assimilation algorithms should be developed through accurate DSD models using observations (e.g., disdrometer or weather radar data) in various climate regimes. Therefore, the uncertainty and sensitivity studies of the parameterizations in the WRF DSD model are critical for extending the data assimilation procedure with DSD, improving the understanding of atmospheric cloud physics, and providing insight into the selection of the DSD models.

The purpose of the present study is to explore the influence of each DSD parameter of the gamma distribution on the accuracy of WRF rainfall simulation by using a ground-based disdrometer located in southern England. Furthermore, the validity of the WRF rain-retrieval algorithm is assessed by evaluating the uncertainty of the WRF rainfall simulation due to the fixed shape parameter in the gamma DSD model. Most of the previous studies on WRF sensitivity analysis have been carried out using several special rainfall events, such as intense storms. However, in this study, the sensitivity of WRF DSD parameterizations is investigated from a long-term perspective by simulating nearly a hundred rainfall events for three different double-moment bulk microphysics schemes. The rainfall events are categorized to different types based on the season, evenness, and

rainfall rate. Moreover, a WRF-disdrometer error assessment approach is developed to validate and analyze the DSD parameterizations of the WRF rainfall retrieval algorithm based on gamma DSD models.

2. Data and models

2.1 Data sources

The Joss-Waldvogel disdrometer (JWD) is a reference instrument for ground DSD measurement that has been widely used to implement the rainfall validation of weather radars or numerical weather forecast models. In this study, an impact-type RD-69 JWD located in Chilbolton Observatory in southern England is selected to evaluate the accuracy and analyze the sensitivity of DSD parameterizations of WRF rainfall simulation. The location (51°08′N, 1°26′W) of the disdrometer is displayed in Figure 1. The JWD data are accessible from April 2003 to September 2017 at the website https://www.chilbolton.stfc.ac.uk and are provided by the British Atmospheric Data Centre (BADC); however, there are several months of missing data. The sampling period and collector area of the disdrometer are 10 s and 50 cm^2, respectively, and drop sizes ranging from 0.3 mm to 5.0 mm were measured with 127 levels.

Preceding studies have found that a short period may lead to counting fluctuations of the observed DSD; however, for a long period, it could smoothen and misrepresent the actual physical variations (Montopoli et al., 2008; Song et al., 2017). Therefore, this study has averaged the JWD raindrop measurements from 10-s periods into 1-min periods to filter out the time variations.

The ERA-Interim dataset produced by ECMWF is used to drive the WRF model in this study. ERA-Interim uses a fixed version of a numerical weather prediction (NWP) system (IFS - Cy31r2) to produce re-analyzed data from 1979 to date. The data can be obtained from http://apps.ecmwf.int/datasets/ with a spatial resolution of approximately 80 km on 60 vertical levels from the surface up to 0.1 hPa. The analyses are available every 6 h (0, 6, 12, and 18 UTC).

A total of 97 rainfall events covering the period from 2013 to 2017 are extracted and simulated from JWD data and the WRF model to analyze the sensitivity of the DSD parameterizations in WRF numerical rainfall prediction. Among the 97 events, 25 rainfall events occurred in the spring season, 13 in summer, 26 in autumn, and 33 in winter.

2.2 The DSD model

The normalized gamma distribution (Equation 1) is generally used as the DSD model of the disdrometer (e.g., JWD) because it allows easy comparisons of the DSD and reduces the DSD uncertainty owing to the absence of restrictions on the shape of raindrop spectra (Bringi et al., 2003; Dai and Han, 2014; Islam et al., 2012; Montopoli et al., 2008).

$$\mathrm{N(D)} = N_w f(\mu) \left(\frac{D}{D_m}\right)^{\mu} \exp\left[-(4+\mu)\frac{D}{D_m}\right], \tag{1}$$

$$f(\mu) = \frac{6(4+\mu)^{\mu+4}}{4^4 \Gamma(\mu+4)}, \tag{2}$$

where $\mathrm{N(D)}$ is the number of raindrops per unit volume, μ is the shape parameter, N_w represents the generalized intercept parameter, D_m is the mass-weighted mean diameter, and $f(\mu)$ is a

function of the shape parameter (Equation 2). The slope and shape parameters are related to the mass-weighted mean diameter by $\lambda D_m = 4 + \mu$. The detailed equations or formulas of the parameters in Equation 1 can be found in Montopoli et al. (2008).

However, for remote-sensing equipment such as weather radars and satellites, the DSD can be retrieved using the measurements of reflectivity Z, and the rainfall rate can be determined with Z-R relations.

The rainfall rate (mm/h) R and reflectivity factor Z are defined in numerical integration forms as follows:

$$\mathrm{R} = 0.6\pi \cdot 10^{-3} \int_0^\infty D^3 V(D) N(D) dD, \tag{3}$$

$$\mathrm{Z} = \int_0^\infty D^6 N(D) dD, \tag{4}$$

where $V(D)$ is the terminal fall speed of raindrops D in mm/s, which is assumed to be $V(D) = 3.67 \cdot D^{0.67}$. The Z-R relationship is generally expressed in the form $\mathrm{Z} = aR^b$, which depends on the DSD characteristics. The coefficients a and b are determined by the atmospheric microphysical properties of the study region and period (Uijlenhoet et al., 2003).

2.3 DSD by the WRF model

The precipitation particle size distribution of the bulk parameterization scheme in the WRF model is treated using a constrained-gamma (CG) distribution model described as follows:

$$\mathrm{N(D)} = N_0 D^\mu e^{-\lambda D}, \tag{5}$$

where μ, N_0, and λ are the shape, intercept, and slope parameters of the raindrop size distribution, respectively; and D is the raindrop diameter. By comparing Equations 1 and 5, the DSD model of the disdrometer can be rewritten in the same format as that of WRF with the following equations.

$$N_0 = \frac{N_w f(u)}{{D_m}^\mu}, \tag{6}$$

$$\lambda = \frac{(4+\mu)}{D_m}, \tag{7}$$

The intercept parameter is an unphysical variable that is equal to the value of $N(D)$ when D is 0 (Tong et al., 2008). For double-moment bulk schemes, the intercept and slope parameters can be extracted from the predicted mixing ratio q and number concentration N as follows:

$$\lambda = \left[\frac{cN\Gamma(\mu + \mathrm{d} + 1)}{q\Gamma(\mu + 1)}\right]^{\frac{1}{d}}, \tag{8}$$

$$N_0 = \frac{N\lambda^{u+1}}{\Gamma(\mu + 1)}, \tag{9}$$

where c and d are the coefficients of an assumed power law between mass and diameter given by $\mathrm{m} = \mathrm{c}D^d$, and $\Gamma(\mathrm{n})$ is the Euler gamma function (Morrison et al., 2009). The double-moment schemes have a fixed value of the shape parameter μ, and most of them set μ to 0, with some exceptions (e.g. the WDM6 schemes, which follow a gamma distribution with μ = 1) (Johnson et

al., 2016; Jung et al., 2010).

2.4 WRF model configuration

The numerical experiment in this study is performed using the WRF model version 3.8 with the Advanced Research WRF dynamical core. By referring to the research results of Liu et al. (2012), triply nested domains centered over the Chilbolton Observatory are designed in this study with a downscaling ratio of 1:3:3. The outer domain (D01) with a grid spacing of 18 km covers the south part of UK, the innermost domain (D03) with the finest grid of 2 km covers the area of interest, and the middle domain (D02) has a grid spacing of 6 km. The distance between each pair of domains is greater than five grid points. With interpolation from the 6-h ECMWF data, the time steps of the three domains are set to 3 h, 1 h, and 15 min, respectively. The domain configuration details are presented in Table 1 and Figure 1. Lambert conformal conic projection is used as the horizontal coordinates of the model. All domains were comprised of 28 vertical pressure levels with the top level set at 50 hPa according to the WRF guidelines. The WRF model runs with longer spin-up times could lead to better rainfall simulation, given better initial weather conditions (Chu et al., 2018). Following the recommendations of previous studies (Chu et al., 2018; Kleczek et al., 2014), a spin-up time of 12 h is adopted for each forecast in the present study to run the WRF model.

By considering that high-resolution NWP forecasts are significantly sensitive to different microphysics parameterizations (Cintineo et al., 2014; Morrison et al., 2015), the current study implements three partially or completely double-moment cloud microphysics schemes to run the WRF model. They were the Morrison double-moment scheme, which predicts the mixing ratios and number concentrations of cloud droplets, cloud ice, snow, rain, and graupel (Morrison et al., 2009); the double-moment 6-class (WDM6) scheme, which adds a prognostic variable to predict the number concentration of cloud condensation nuclei (CCN) (Hong et al., 2010; Lim and Hong, 2010); and the Thompson aerosol-aware scheme, which predicts the number concentrations of both CCN and ice nuclei (IN) (Thompson and Eidhammer, 2014).

The other physics parameterizations used are the following. For the cumulus scheme, which is a significant factor for rainfall simulation, a simple and efficient method called the Kain–Fritsch scheme (Kain, 2004) is used, but the cumulus scheme not used in the innermost domain, where the convective rainfall generation is assumed to be definitely resolved (Liu et al., 2012). For the planetary boundary-layer scheme, which has a strong relationship with the spatial distribution of rainfall and temperature, the Mellor-Yamada-Janjic method (Janjić, 1994), broadly used in the WRF simulation (Evans et al., 2012; Awan et al., 2011), is adopted. The radiation processes include the RRTM scheme for longwave radiation (Mlawer et al., 1997) and Dudhia scheme for shortwave Radiation (Dudhia, 1989). The Noah land-surface model (Ek et al., 2003) is selected coupled with the Monin–Obukhov scheme, which is used for the description of the surface layer (Monin and Obukhov, 1954).

3. Scenarios and experimental designs

This study investigates the sensitivity of DSD parameterizations of the WRF model by using three double-moment microphysics schemes: Morrison, WDM6, and Thompson aerosol-aware. The studied rainfall events simulated by each microphysics scheme are categorized into 12 scenarios

based on the season, evenness, and rainfall rate which have not been explored in other studies. They are scenarios A1–A4: spring rain, summer rain, autumn rain, and winter rain by season; scenarios B1–B2: even rain and uneven rain by evenness; and scenarios C1–C6: R = (0.1, 0.2], (0.2, 0.4], (0.4, 0.8], (0.8, 1.6], (1.6, 3.2], and R>3.2 mm/h by rainfall rate.

Even and uneven rain are distinguished on the basis of the temporal evenness of rainfall distribution by using the two most frequently used variability indices: coefficient of variability (CV) and variability index (VI) (Liu et al., 2012; Van Etten, 2009). CV and VI are described by the following equations:

$$\mathrm{CV} = \sqrt{\frac{1}{M}\sum_{i=1}^{M}\left(\frac{x_i}{\bar{x}} - 1\right)^2}, \tag{10}$$

$$\mathrm{VI} = \frac{90th\% - 10th\%}{50th\%}, \tag{11}$$

where x_i is the rainfall at time step i for a certain rainfall event; $\bar{x}$ represents the mean value of x_i; M is the total number of time steps of each rainfall event; and 90^{th}%, 10^{th}%, and 50^{th}% are percentiles of the x_i series. Larger values of CV and VI indicate a rainfall distribution with greater variability.

The main principle of the sensitivity analysis of DSD parameterizations is to quantify and compare changes in results by shifting the parameterizations up or down to different degrees within a reasonably constrained interval. The potential constrained interval of the parameterizations in the WRF DSD model is calculated through the ground-based disdrometer data in this study. Through Equations 1, 5, 6, and 7, the DSD parameter values of μ, N_0, and λ of the disdrometer can be calculated for each minute of the studied rainfall events. Thus, the potential constrained interval and floating range for the sensitivity analysis of WRF DSD parameterizations can be obtained. The corresponding results are elaborated in Section 4.1.

In addition, three error indices, namely the probability of detection (POD), root-mean-square error (RMSE), and mean bias error (MBE) (Dai et al., 2015) were selected to evaluate the performance and analyze the sensitivity of DSD parameterizations of the WRF model for rainfall of different seasons and evenness types. The POD is a categorical index that generally evaluates the simulation accuracy on the basis of the correctness of rainfall occurrence, whereas RMSE and MBE are continuous verification indices that provide a more quantitative calculation of the simulation error (Jolliffe and Stephenson, 2003; Liu et al., 2012).

The POD is the ratio between the time steps in which the WRF simulated rainfall matches the observed disdrometer rainfall and the total time steps of the whole rainfall event with a threshold of 0.1 mm, as described by Equation 12. The value of POD ranges from 0 to 1, and a large value indicates a high degree of rainfall detection. We adopt these metrics to explore the influence level of the variations of DSD parameters on the rainfall recognition rate.

$$\mathrm{POD} = \frac{R_d}{R_d + R_n}, \tag{12}$$

where R_d represents the number of time steps in which the simulated rainfall matched the

disdrometer rainfall and R_n denotes the number of time steps in which the simulated rainfall missed the rainfall detected by the disdrometer.

RMSE is the square root of the average of squared errors, and it is a frequently used index to measure the differences between the simulated or predicted values and the observed values. This metric is selected to quantify the influence of the variation of the DSD parameter on the accuracy of rainfall estimation. RSME ranges from 0 to infinity, and a lower RMSE indicates a better fit to the observed data. MBE measures the average overestimation or underestimation of the cumulative rainfall with a perfect score of 0. This index is used to investigate the deviation direction and extent when the parameters are shifted or adjusted. Those two indices can be derived through the following equations:

$$\mathrm{RMSE} = \sqrt{\frac{1}{N}\sum_{i=1}^{N}(W_i - D_i)^2}, \tag{13}$$

$$\mathrm{MBE} = \frac{1}{N}\sum_{i=1}^{N}(W_i - D_i), \tag{14}$$

where W_i and D_i are the rainfall accumulations of each rainfall event at time *i* obtained from the WRF DSD and disdrometer DSD, respectively. Further, N is the total number of rainfall events.

To clearly describe the direction at which the estimated data or adjusted data deviates from the observed data, this study normalizes MBE into the range of -1 to 1. The value -1 implies that the average value of W_i is 0, while 1 represents the maximum value of those MBEs greater than 0 in each WRF microphysics scheme with respect to different WRF DSD parameterizations.

Moreover, we use relative bias to explore the sensitivity of the DSD parameterizations at different rainfall rates as follows:

$$\sigma_R = \sum_{i=1}^{N}\frac{(W_i - D_i)}{W_i}. \tag{15}$$

In Equation 15, W_i and D_i are the WRF and disdrometer rainfall rates (R > 0.1 mm/h), respectively, at the time step *i* within six rainfall rate intervals (C1–C6), and N is the total number of time steps.

4. Results and discussion

4.1 Potential constrained intervals for sensitivity analysis of DSD parameterizations

The potential constrained intervals used for the sensitivity analysis of DSD parameterizations are derived from the disdrometer data of the studied rainfall events. Since the shape parameter (μ) of DSD in WRF double-moment schemes is fixed, the intercept (N_0) and slope (λ) parameters of the disdrometer DSD are calculated under the same condition. The probability density functions (PDFs) of μ, $log_{10}N_0$, and λ of the disdrometer are presented in Figure 2. All three parameters have large ranges: μ ranges from approximately -2.3 to 60 with a median of 5.6, $log_{10}N_0$ ranges from 1.3 to 5.5 with a median of 3.9, and λ ranges from 1.0 to 11.7 with a median of 4.6. In view of the large

ranges of these parameters, the current study does not include the values with small probabilities in the variation range for the sensitivity analysis of WRF DSD parameterizations; rather, the floated values are limited within the minimum and maximum of the disdrometer parameters.

The potential variation ranges are the grey parts displayed in Figure 2, which are the middle 90% values of each parameter. The potential constrained ranges are approximately 0 to 33 for μ, 3.2 to 5.1 for $log_{10}N_0$, and 2.8 to 9.7 for λ. Combining the potential constrained ranges with the median values, the range and interval of each parameter include the following (Table 2): setting the μ range from 0 to 33 with an interval of 1; reducing the value of $log_{10}N_0$ to 18% with an interval of 2% and increasing the value up to 31% in the same manner; and for λ, the floating scope is from -40% to +110% with an interval of 5%. For simplicity, in this paper, we use the negative sign to indicate that the values of parameters are reduced, and the positive sign implies that the values are increased. The boundary conditions of $log_{10}N_0$ are 1.3 and 5.5 and of λ are 1.0 and 11.7, respectively.

4.2 The WRF and disdrometer DSD retrieval

The WRF model downscales the ERA-Interim data for each rainfall event and obtains DSD data and parameters by using the Morrison, WDM6, and Thompson aerosol-aware schemes. The DSD parameters for the disdrometer are also calculated for the same rainfall events. The minimum, median, and maximum of the $log_{10}N_0$ and λ of the disdrometer and WRF DSD are listed in Table 3. The parameters of the WRF model, especially λ, show a wider range than those of the disdrometer. However, the WDM6 scheme has a larger scope than the other schemes and shows a high median deviation from the disdrometer, while the Thompson aerosol-aware scheme acquires similar medians; further, the Thompson aerosol-aware scheme and Morrison scheme have a smaller parameter range.

Figure 3 shows the Z-R relations obtained from the WRF simulation DSD results of the three microphysics schemes (Z_w-R_w, blue scatters and lines) and disdrometer observational data (Z_o-R_o, red scatters and lines). The coefficient b is similar to a large extent between the Morrison scheme and disdrometer data, and the coefficient a of the Thompson aerosol-aware scheme is close to that of the disdrometer data. However, the similarity between the WDM6 scheme and disdrometer data is relatively poor.

Further, the WRF simulation results of three microphysics schemes using the fixed-μ gamma distribution with μ equal to 0 (Morrison and Thompson aerosol-aware schemes) or 1 (WDM6 scheme) are compared to the rainfall observed using the disdrometer DSD model in terms of POD, RMSE, and MBE. Table 4 compares the POD, RMSE, and MBE values of the three schemes in the four seasons and for even and uneven rain; the values are calculated from the disdrometer and WRF DSD results. All rainfall events are divided into even and uneven rain (42% and 58% of the total rainfall events, respectively) by setting the threshold of CV as 4.0 and that of VI as 10.0.

The Thompson aerosol-aware scheme obtained the highest accuracy in most cases. However, the upper limit in the Thompson aerosol-aware scheme, as shown in Figure 3, could influence the model evaluation statistics (POD, RMSE, and MBE); i.e., underestimation is caused by the elimination of higher values. We believe that this could be one of the reasons why the Thompson aerosol-aware scheme obtained the best performance overall among the studied schemes. That is, for scenarios with the detailed classification of rainfall, apart from the several scenarios designed in this paper,

the best-performing schemes may be flexible.

A comparison of the rainfall of the four seasons shows that the difference among seasons is not clearly distinguished, even though the winter rainfall has the lowest RMSE and the summer rainfall is underestimated slightly for all schemes. However, the results of comparing even and uneven rain indicate that the WRF model provides accurate rainfall simulation for even rain with a large value of POD and small values of RMSE and MBE.

The relative biases in different rainfall rates of the three microphysics schemes are listed in Table 5. All schemes overestimate light rain (C1–C4), whereas heavy rain (C5 and C6) is underestimated. Furthermore, the relative bias of light rain (C1–C3) is more pronounced than that of heavy rain (C4–C6). In addition, the Thompson aerosol-aware scheme performs better than the Morrison and WDM6 schemes in C1–C4.

4.3 DSD parameterization sensitivity in different situations

The POD indices are used to evaluate the influence of different DSD parameterizations on the ability to capture rainfall events. Figure 4 shows the results of DSD parameterization sensitivity according to the POD indices of the three microphysics schemes with μ ranging from 0 to 33, $log_{10}N_0$ ranging from -18% to +33%, and λ ranging from -40% to +110% in the four seasons and for even and uneven rain. Overall, the sensitivity patterns of the DSD parameterizations according to the POD indices for different microphysics schemes are similar, but in most cases, the DSD parameterizations of the WDM6 scheme show lower sensitivity compared to the Morrison and Thompson aerosol-aware schemes. The POD indices exhibit a small variation when the parameters μ and λ are changed, but they vary greatly as the value of $log_{10}N_0$ is adjusted. The POD indicator is easier to be influenced by the parameter variation of even rain compared to uneven rain for different microphysics schemes. In contrast, the sensitivity differences of the DSD parameterizations among the four seasons are not significant.

For parameter μ, POD increased slightly when the value of μ increased beyond approximately 10, but with some exceptions. For N_0, POD increased slowly as the value of $log_{10}N_0$ decreased, and it increased faster as $log_{10}N_0$ decreased further until a turning point (approximately +15%). For λ, POD decreased briefly as λ increased, but the magnitude of the change is insignificant.

To evaluate the influence of different WRF DSD parameterizations on the quantification error of WRF rainfall retrieval, the RMSE indicator is adopted and calculated for three different microphysics schemes. The corresponding results of RMSE derived from DSD gamma distributions with a series of μ, $log_{10}N_0$, and λ values for four seasons as well as even and uneven rain are presented in Figure 5. In terms of RMSE, the trends are similar across the three schemes, but the DSD parameterizations of the WDM6 scheme exhibit the highest sensitivity. Moreover, RMSE is significantly more susceptible to $log_{10}N_0$ compared to the other parameters. RMSE is slightly less sensitive to the parameters of even rain for the three schemes, and even rain results in smaller values of RMSE compared to uneven rain. Additionally, from the results of RMSE, the discrepancies in the sensitivity of the WRF DSD model to the parameters among different seasons are not clear.

For parameter μ, a significant increase in RMSE occurs when μ increases beyond a threshold (approximately 13 for Morrison and Thompson aerosol-aware schemes and approximately 10 for WDM6). In contrast, the RMSE shows small variation when μ is less than the threshold. In the case

of N_0, RMSE increased greatly as $log_{10}N_0$ decreased or increased. The trend for λ is similar to that for $log_{10}N_0$ but with a lower RMSE variation.

To further investigate the bias direction of WRF rainfall simulation when adjusting WRF DSD parameters, the normalized MBE is calculated. The normalized MBE results of each parameter for different seasons, evenness types, and schemes are shown in Figure 6. Again, the sensitivity trend on the basis of the normalized MBE to each parameter is similar for different microphysics schemes. In the part where the WRF rainfall is underestimated (normalized MBE < 0), the results of $log_{10}N_0$ express the largest sensitivity followed by those of λ and μ. However, in the underestimated part, the difference in the sensitivity based on the normalized MBE to different parameters cannot be distinguished, because the MBE values are normalized by its maximum value for each microphysics scheme and parameter when MBE is greater than 0. MBE is more sensitive to the DSD parameters of uneven rainfall events, for which the WRF DSD calculated rainfall is overestimated. In addition, the MBE seems to be less sensitive to the DSD parameters of autumn compared to those of the other seasons.

The overall rainfall tends to be underestimated (normalized MBE < 0) first and then overestimated (normalized MBE>0) as the value of μ increases. However, for $log_{10}N_0$ and λ, the WRF rainfall is overestimated progressively as the value reduces and underestimated gradually as the value increases. The results also indicate that the underestimation degree of WRF rainfall for $log_{10}N_0$ is greater than that for λ when the value is increased, as can be verified by the POD results.

The sensitivity of DSD parameterizations is explored for different rainfall rates by relative bias as well. Figure 7 shows the relative biases of all time steps of different DSD parameterizations for six rainfall-rate intervals (scenarios C1–C6) and three microphysics schemes. The sensitivity trends for those rainfall-rate intervals with respect to different DSD parameterizations are similar, and the results of the WDM6 scheme show a higher sensitivity compared to the Morrison and Thompson aerosol-aware schemes. For a detailed comparison of different rainfall rates, it is evident that the sensitivity to each parameter decreases as the rainfall intensity increases. Light rain is greatly overestimated with a rapid growth when μ is greater than approximately 10–15, and $log_{10}N_0$ and λ are decreased in comparison with heavy rainfall.

4.4 Uncertainty of WRF rainfall estimation caused by DSD shape parameter

It is clear from Section 4.3 that the μ parameter has a turning point, and the sensitivity stays low when the value of μ is less than this point, which indicates that the fixed-μ gamma DSD model is probably not the optimal option. Therefore, in this section, the values of μ less than or around the turning points are analyzed separately for the three microphysics schemes and different rainfall evenness types and rates (rainfall events classified by season are not included because the sensitivity differences among the four seasons are not significant) to investigate the uncertainty of WRF rainfall retrievals caused by μ.

The POD, RMSE and MBE derived from the gamma DSD model with μ ranging from 0 to 14 for the three microphysics schemes and two types of rain are compared and contrasted in Figure 8. The variation of the POD for uneven rain is increased slightly with a larger μ, which suggests that the explored values have a small impact on the rainfall detection rate for uneven rain. However, the values of the POD for even rain are significantly influenced by μ, especially for the WDM6 scheme,

with the trend of an initial decrease followed by an increase as the value of μ increases. Remarkably, in this case, the difference of POD between μ values of 0 and 14 is insignificant, and a μ value of 0 exhibits a better performance than many values of μ. From the results of POD, a fixed-μ gamma DSD model with μ equal to 0 is suitable as well as the WDM6 scheme, which adopted μ equal to 1.

For RMSE, the turning point of uneven rain is earlier than that of even rain, and both of them show two valleys of RMSE among the study values of μ. As shown in the middle plots of Figure 8, the turning points are 10 (uneven rain) and 12 (even rain) for Morrison, 8 (uneven and even rain) for WDM6, and 10 (uneven rain) and 13 (even rain) for Thompson aerosol-aware. Obviously, the turning point is one of the minima, and the value 1 or 2 is another minimum. The RMSE of the turning point seems to have a smaller value than that of the first valley in most instances. However, the turning point cannot be fixed. For example, the turning point of WDM6 is smaller than those of the other two, and uneven rain shows a smaller value of the turning point. That is, the turning point could be determined by many factors apart from rainfall type and microphysics scheme. Nevertheless, the RMSE obtained from μ = 0 is higher than those obtained from most values below the turning point for Morrison and Thompson aerosol-aware schemes, but the performance at μ = 1 for WDM6 is suitable. In general, the comparisons of RMSE for different μ values clearly imply that values around the turning point yield the best accuracy, followed by μ = 1 or 2.

The best accuracy points illustrated by MBE are close to the case of RMSE, but with some exceptions. The best performance point of MBE is μ = 1 for even rain and μ = 12 for uneven rain for the Morrison scheme, μ= 8 for the WDM6 scheme, and μ = 0 for even rain and μ=12 for uneven rain for the Thompson aerosol-aware scheme. It is noteworthy that, for the Morrison and Thompson aerosol-aware schemes, the turning points of RMSE exhibit an underestimation of rainfall, and the values around the turning point of RMSE that show the lowest bias seem to be the values greater than the turning point. However, for WDM6, the values that yield the smallest deviation are the same as the optimal values of RMSE.

The above analysis reveals that the values of turning points are a preferable option for obtaining an excellent POD and RMSE, but for the purpose of obtaining a smaller error or bias, we believe that μ equal to 1 is a good choice as well. However, the turning points are uncertain in different situations. Therefore, to balance all indices, we recommend a fixed-μ gamma DSD model with μ equal to 1 for uneven rain and 0 for even rain for all the studied microphysics schemes, supposing that the set of turning points of different scenarios is difficult to calculate.

In addition, the uncertainty of the WRF rainfall simulation due to the DSD shape parameter has also been explored for different rainfall rates. Combined with the constrained intervals of the shape parameter derived from disdrometer data for different rainfall rates, the optimal μ values that yield the smallest relative bias of different rainfall rates are shown in Figure 9. For the Morrison scheme, the optimal value of the shape parameter deceased as the rainfall rate increased; while for the WDM6 and Thompson aerosol-aware schemes, the optimal value deceased first and then increased as the rainfall rate increased. The optimal values of different rainfall rates demonstrate that the fixed-μ gamma DSD model with μ equal to 0 or 1 is not the perfect model for WRF rainfall retrieval with the studied microphysics schemes. The results suggest that an adaptive-μ gamma model should be adopted, and the value of μ could be determined according to the rainfall rate and microphysics scheme. That is, by using validation data such as disdrometer data, some intelligent optimization

algorithms for the shape parameter could be developed based on the rainfall rate, microphysics parameterization, and so on.

5. Conclusion

This study assessed the accuracy, sensitivity, and uncertainty of the DSD parameterizations of the gamma distribution employed in WRF numerical weather prediction models through comparison with observed disdrometer DSD data. Three double-moment microphysics schemes with different levels of complexity were adopted, and 97 simulation rainfall events were categorized into 12 scenarios based on the season, evenness, and rainfall rate. Analysis results reveal the following.

1. The Thompson aerosol-aware microphysics parameterization showed the best performance with a higher rainfall recognizability, smaller accumulation and intensity errors, and smaller biases compared to the Morrison and WDM6 schemes in the studied climatological regimes. The seasonal difference in WRF rainfall retrieval was not distinct. The even rain simulated by WRF resulted in a significantly higher accuracy compared to uneven rain. On the other hand, the simulated precipitation with a low rate has a larger relative bias compared to that with a high rate, and the WRF model overestimated low rainfall rates while underestimating high rainfall rates.

2. Among the three DSD parameters, the variation of the intercept parameter N_0 has the greatest influence on the WRF simulated rainfall. In contrast, the sensitivity of the WRF DSD parameterizations to the shape parameter μ and slope parameter λ is relative small. As the value of μ increases, the rainfall tended to be underestimated first and then overestimated. For parameters $log_{10}N_0$ and λ, the WRF simulated rainfall is overestimated when they decrease and underestimated when they increase and then stay constant.

3. The DSD model sensitivity pattern of each parameter are similar for the three microphysics schemes. The sensitivity of the DSD parameterizations shows no significant difference among seasons for all three parameters. The parameters of even rain have a higher influence on the ability to capture rainfall events but a lower variation of errors and biases compared to those of uneven rain. In addition, the simulated precipitation with a low rate is easier to be affected by the variation of the gamma DSD model parameter than with a high rate.

4. The results also suggest that the gamma DSD model with a fixed μ is not the optimal setting. A gamma DSD model with an adaptive value of μ should be developed based on the evenness, rainfall rate, and microphysics scheme by using the WRF model. Supposing that the adaptive value of μ is difficult to calculate, this study recommends a fixed-μ gamma DSD model with μ equal to 1 for uneven rain and 0 for even rain.

The potential constrained intervals used for investigating the parameter sensitivity of the gamma DSD model are obtained from the disdrometer DSD parameter range. However, this study does not consider that different rainfall rates may yield different widths of the range, which means that the potential constrained intervals used in this study is probably wider than the actual interval. Further work will aim to rectify this issue. Another limitation of the study is the discrepancy between the spatial coverages of the disdrometer and WRF grid under the assumption of the representativeness of the disdrometer over the whole WRF grid (this assumption can be assumed as sufficient owing

to the small WRF grid size). Moreover, owing to the data limitations and time required for WRF operation, this study is conducted only in southern England; therefore, the results of this study might not be representative of the catchments of different geographic and climatic conditions. We hope that this experiment would be replicated in more regions in the future. In combination with the sensitivity analysis of the WRF DSD parameterizations, future studies will aim to develop an adaptive-μ gamma DSD model and explore some linear/nonlinear regression methods to correct WRF DSD and improve the accuracy of WRF rainfall retrievals by assimilating observation data (e.g., disdrometer data).

Acknowledgements

This study was supported by the National Natural Science Foundation of China (Nos. 41771424, 41871299), Newton Fund via the Natural Environment Research Council (NERC) and Economic and the Social Research Council (ESRC) (NE/N012143/1), the University Natural Science Project of Jiangsu Province (No. 16KJA170001), and the National Key R & D Program of China (Nos. 2018YFB0505500, 2018YFB0505502). This authors acknowledge the Advanced Computing Research Centre at the University of Bristol for proving access to the High-Performance Computing (HPC) system BlueCrystal.

Reference

Angulo-Martínez, M., Beguería, S., Kyselý, J., Use of disdrometer data to evaluate the relationship of rainfall kinetic energy and intensity (KE-I), *Science of the Total Environment* **568**(2016), pp. 83-94.

Awan, N.K., Truhetz, H., Gobiet, A., Parameterization-Induced Error Characteristics of MM5 and WRF Operated in Climate Mode over the Alpine Region: An Ensemble-Based Analysis, *Journal of Climate* **24**(2011), pp. 3107-3123.

Bringi, V. *et al.*, Raindrop size distribution in different climatic regimes from disdrometer and dual-polarized radar analysis, *Journal of the atmospheric sciences* **60**(2003), pp. 354-365.

Bringi, V., Huang, G.-J., Chandrasekar, V., Gorgucci, E., A methodology for estimating the parameters of a gamma raindrop size distribution model from polarimetric radar data: Application to a squall-line event from the TRMM/Brazil campaign, *Journal of Atmospheric and Oceanic Technology* **19**(2002), pp. 633-645.

Brown, B.R., Bell, M.M., Frambach, A.J., Validation of simulated hurricane drop size distributions using polarimetric radar, *Geophysical Research Letters* **43**(2016), pp. 910-917.

Chu, Q., Xu, Z., Chen, Y., Han, D., Evaluation of the ability of the Weather Research and Forecasting model to reproduce a sub-daily extreme rainfall event in Beijing, China using different domain configurations and spin-up times, *Hydrology and Earth System Sciences* **22**(2018), p. 3391.

Cintineo, R., Otkin, J.A., Xue, M., Kong, F., Evaluating the performance of planetary boundary layer and cloud microphysical parameterization schemes in convection-permitting ensemble forecasts using synthetic GOES-13 satellite observations, *Monthly Weather Review* **142**(2014),

pp. 163-182.

Ćurić, M., Janc, D., Veljović, K., Dependence of accumulated precipitation on cloud drop size distribution, *Theoretical and applied climatology* **102**(2010), pp. 471-481.

Ćurić, M., Janc, D., Vučković, V., Kovačević, N., The impact of the choice of the entire drop size distribution function on Cumulonimbus characteristics, *Meteorologische Zeitschrift* **18**(2009), pp. 207-222.

Dai, Q., Han, D., Exploration of discrepancy between radar and gauge rainfall estimates driven by wind fields, *Water Resources Research* **50**(2014), pp. 8571-8588.

Dai, Q., Rico-Ramirez, M.A., Han, D., Islam, T., Liguori, S., Probabilistic radar rainfall nowcasts using empirical and theoretical uncertainty models, *Hydrological processes* **29**(2015), pp. 66-79.

Dawson, D.T., Xue, M., Milbrandt, J.A., Yau, M., Comparison of evaporation and cold pool development between single-moment and multimoment bulk microphysics schemes in idealized simulations of tornadic thunderstorms, *Monthly Weather Review* **138**(2010), pp. 1152-1171.

Dudhia, J., Numerical study of convection observed during the winter monsoon experiment using a mesoscale two-dimensional model, *Journal of the atmospheric sciences* **46**(1989), pp. 3077-3107.

Ek, M. *et al.*, Implementation of Noah land surface model advances in the National Centers for Environmental Prediction operational mesoscale Eta model, *Journal of Geophysical Research: Atmospheres* **108**(2003).

Evans, J.P., Ekström, M., Ji, F., Evaluating the performance of a WRF physics ensemble over South-East Australia, *Climate Dynamics* **39**(2012), pp. 1241-1258.

Gilmore, M.S., Straka, J.M., Rasmussen, E.N., Precipitation uncertainty due to variations in precipitation particle parameters within a simple microphysics scheme, *Monthly weather review* **132**(2004), pp. 2610-2627.

Han, M., Braun, S.A., Matsui, T., Williams, C.R., Evaluation of cloud microphysics schemes in simulations of a winter storm using radar and radiometer measurements, *Journal of Geophysical Research: Atmospheres* **118**(2013), pp. 1401-1419.

Hong, S.-Y. *et al.*, Evaluation of the WRF double-moment 6-class microphysics scheme for precipitating convection, *Advances in Meteorology* **2010**(2010).

Iguchi, T., Matsui, T., Tokay, A., Kollias, P., Tao, W.K., Two distinct modes in one-day rainfall event during MC3E field campaign: Analyses of disdrometer observations and WRF-SBM simulation, *Geophysical Research Letters* **39**(2012).

Islam, T., Rico-Ramirez, M.A., Thurai, M., Han, D., Characteristics of raindrop spectra as normalized gamma distribution from a Joss–Waldvogel disdrometer, *Atmospheric Research* **108**(2012), pp. 57-73.

Janjić, Z.I., The step-mountain eta coordinate model: Further developments of the convection, viscous sublayer, and turbulence closure schemes, *Monthly Weather Review* **122**(1994), pp. 927-945.

Johnson, M., Jung, Y., Dawson, D.T., Xue, M., Comparison of simulated polarimetric signatures in idealized supercell storms using two-moment bulk microphysics schemes in WRF, *Monthly Weather Review* **144**(2016), pp. 971-996.

Jolliffe, I.T., Stephenson, D.B., *Forecast verification: a practitioner's guide in atmospheric science*. John Wiley & Sons (2003).

Jung, Y., Xue, M., Zhang, G., Simulations of polarimetric radar signatures of a supercell storm using a two-moment bulk microphysics scheme, *Journal of Applied Meteorology and Climatology* **49**(2010), pp. 146-163.

K'ufre-Mfon, E.E., Hunt, F.H., Jeffery, J.L., Otung, I.E., Modeling rainfall drop size distribution in southern England using a Gaussian Mixture Model, *Radio Science* **50**(2015), pp. 876-885.

Kain, J.S., The Kain–Fritsch Convective Parameterization: An Update, *Journal of Applied Meteorology* **43**(2004), pp. 170-181.

Kala, J., Andrys, J., Lyons, T.J., Foster, I.J., Evans, B.J., Sensitivity of WRF to driving data and physics options on a seasonal time-scale for the southwest of Western Australia, *Climate dynamics* **44**(2015), pp. 633-659.

Khain, A., Lynn, B., Shpund, J., High resolution WRF simulations of Hurricane Irene: Sensitivity to aerosols and choice of microphysical schemes, *Atmospheric Research* **167**(2016), pp. 129-145.

Kirankumar, N., Rao, T.N., Radhakrishna, B., Rao, D.N., Statistical characteristics of raindrop size distribution in southwest monsoon season, *Journal of Applied Meteorology and Climatology* **47**(2008), pp. 576-590.

Kleczek, M.A., Steeneveld, G.-J., Holtslag, A.A.M., Evaluation of the Weather Research and Forecasting Mesoscale Model for GABLS3: Impact of Boundary-Layer Schemes, Boundary Conditions and Spin-Up, *Boundary-Layer Meteorology* **152**(2014), pp. 213-243.

Kogan, Y.L., Belochitski, A., Parameterization of cloud microphysics based on full integral moments, *Journal of the Atmospheric Sciences* **69**(2012), pp. 2229-2242.

Lim, K.-S.S., Hong, S.-Y., Development of an effective double-moment cloud microphysics scheme with prognostic cloud condensation nuclei (CCN) for weather and climate models, *Monthly weather review* **138**(2010), pp. 1587-1612.

Lin, Y.-L., Farley, R.D., Orville, H.D., Bulk Parameterization of the Snow Field in a Cloud Model, *Journal of Climate and Applied Meteorology* **22**(1983), pp. 1065-1092.

Liu, J., Bray, M., Han, D., Sensitivity of the Weather Research and Forecasting (WRF) model to downscaling ratios and storm types in rainfall simulation, *Hydrological Processes* **26**(2012), pp. 3012-3031.

Meshesha, D.T., Tsunekawa, A., Tsubo, M., Haregeweyn, N., Tegegne, F., Evaluation of kinetic energy and erosivity potential of simulated rainfall using Laser Precipitation Monitor, *Catena* **137**(2016), pp. 237-243.

Milbrandt, J., Yau, M., A multimoment bulk microphysics parameterization. Part IV: Sensitivity

experiments, *Journal of the atmospheric sciences* **63**(2006), pp. 3137-3159.

Milbrandt, J.A., Yau, M.K., A Multimoment Bulk Microphysics Parameterization. Part I: Analysis of the Role of the Spectral Shape Parameter, *Journal of the Atmospheric Sciences* **62**(2005), pp. 3051-3064.

Mlawer, E.J., Taubman, S.J., Brown, P.D., Iacono, M.J., Clough, S.A., Radiative transfer for inhomogeneous atmospheres: RRTM, a validated correlated-k model for the longwave, *Journal of Geophysical Research: Atmospheres* **102**(1997), pp. 16663-16682.

Monin, A., Obukhov, A., Basic laws of turbulent mixing in the surface layer of the atmosphere, *Contrib. Geophys. Inst. Acad. Sci. USSR* **151**(1954), p. e187.

Montopoli, M., Marzano, F.S., Vulpiani, G., Analysis and synthesis of raindrop size distribution time series from disdrometer data, *IEEE Transactions on Geoscience and Remote Sensing* **46**(2008), pp. 466-478.

Morrison, H. *et al.*, Parameterization of cloud microphysics based on the prediction of bulk ice particle properties. Part II: Case study comparisons with observations and other schemes, *Journal of the Atmospheric Sciences* **72**(2015), pp. 312-339.

Morrison, H., Pinto, J., Mesoscale modeling of springtime Arctic mixed-phase stratiform clouds using a new two-moment bulk microphysics scheme, *Journal of the atmospheric sciences* **62**(2005), pp. 3683-3704.

Morrison, H., Thompson, G., Tatarskii, V., Impact of cloud microphysics on the development of trailing stratiform precipitation in a simulated squall line: Comparison of one-and two-moment schemes, *Monthly Weather Review* **137**(2009), pp. 991-1007.

Shrestha, R.K., Connolly, P.J., Gallagher, M.W., Sensitivity of WRF cloud microphysics to simulations of a convective storm over the Nepal Himalayas, *The Open Atmospheric Science Journal* **11**(2017).

Song, Y., Han, D., Rico-Ramirez, M.A., High temporal resolution rainfall rate estimation from rain gauge measurements, *Journal of Hydroinformatics* **19**(2017), pp. 930-941.

Tapiador, F.J., Checa, R., de Castro, M., An experiment to measure the spatial variability of rain drop size distribution using sixteen laser disdrometers, *Geophysical Research Letters* **37**(2010).

Thompson, G., Eidhammer, T., A study of aerosol impacts on clouds and precipitation development in a large winter cyclone, *Journal of the atmospheric sciences* **71**(2014), pp. 3636-3658.

Tong, M., Xue, M., Simultaneous Estimation of Microphysical Parameters and Atmospheric State with Simulated Radar Data and Ensemble Square Root Kalman Filter. Part I: Sensitivity Analysis and Parameter Identifiability, *Monthly Weather Review* **136**(2008), pp. 1630-1648.

Uijlenhoet, R., Steiner, M., Smith, J.A., Variability of raindrop size distributions in a squall line and implications for radar rainfall estimation, *Journal of Hydrometeorology* **4**(2003), pp. 43-61.

Van Etten, E.J., Inter-annual rainfall variability of arid Australia: greater than elsewhere?, *Australian Geographer* **40**(2009), pp. 109-120.

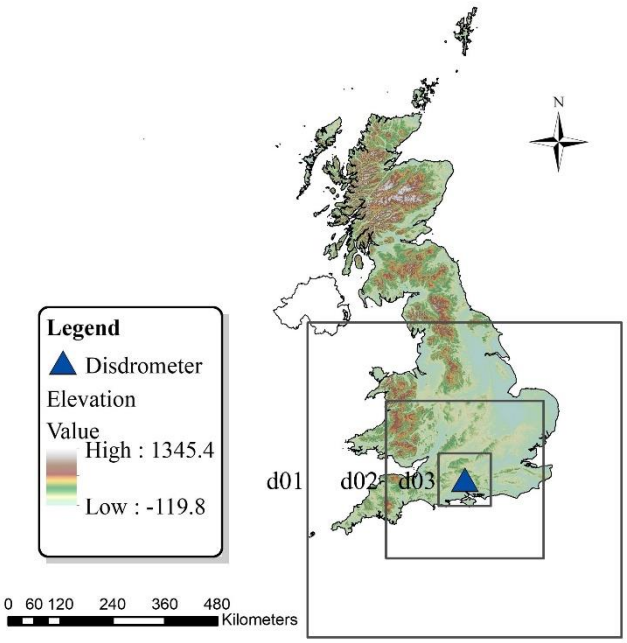

Figure 1. Location of the JWD at Chilbolton Observatory and the domain configurations in the WRF model.

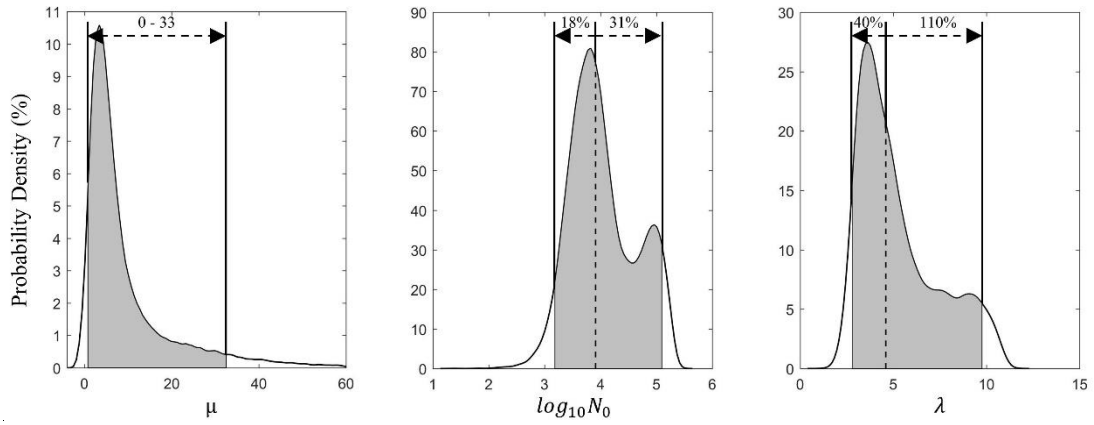

Figure 2. PDF of disdrometer DSD parameters resulting from the studied rainfall events. The grey area includes the middle 90% values of each parameter, and the black dotted line represents the median value of the parameter.

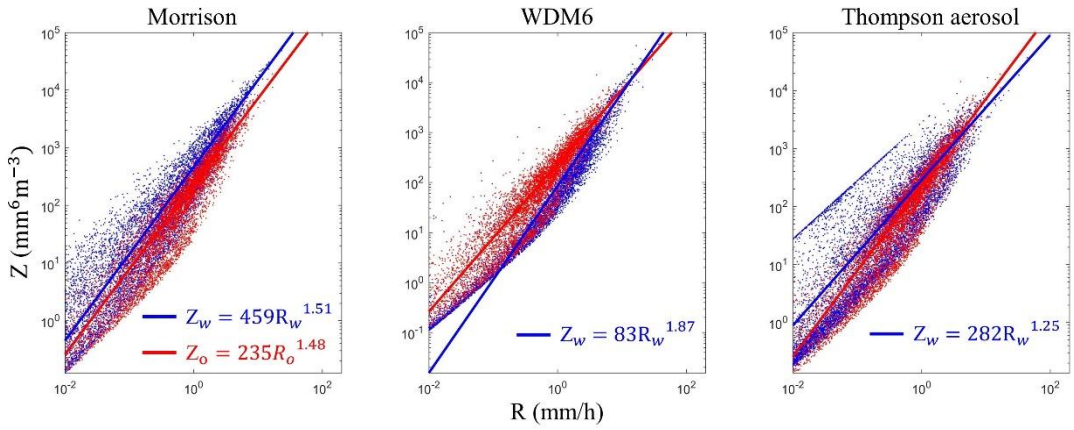

Figure 3. Scatter diagrams between Z and R derived from the disdrometer observational data (o) and the WRF simulation DSD results of three microphysics schemes (w). The blue scatters and lines show the WRF results (w), and the red scatters and lines represent the observational results (o).

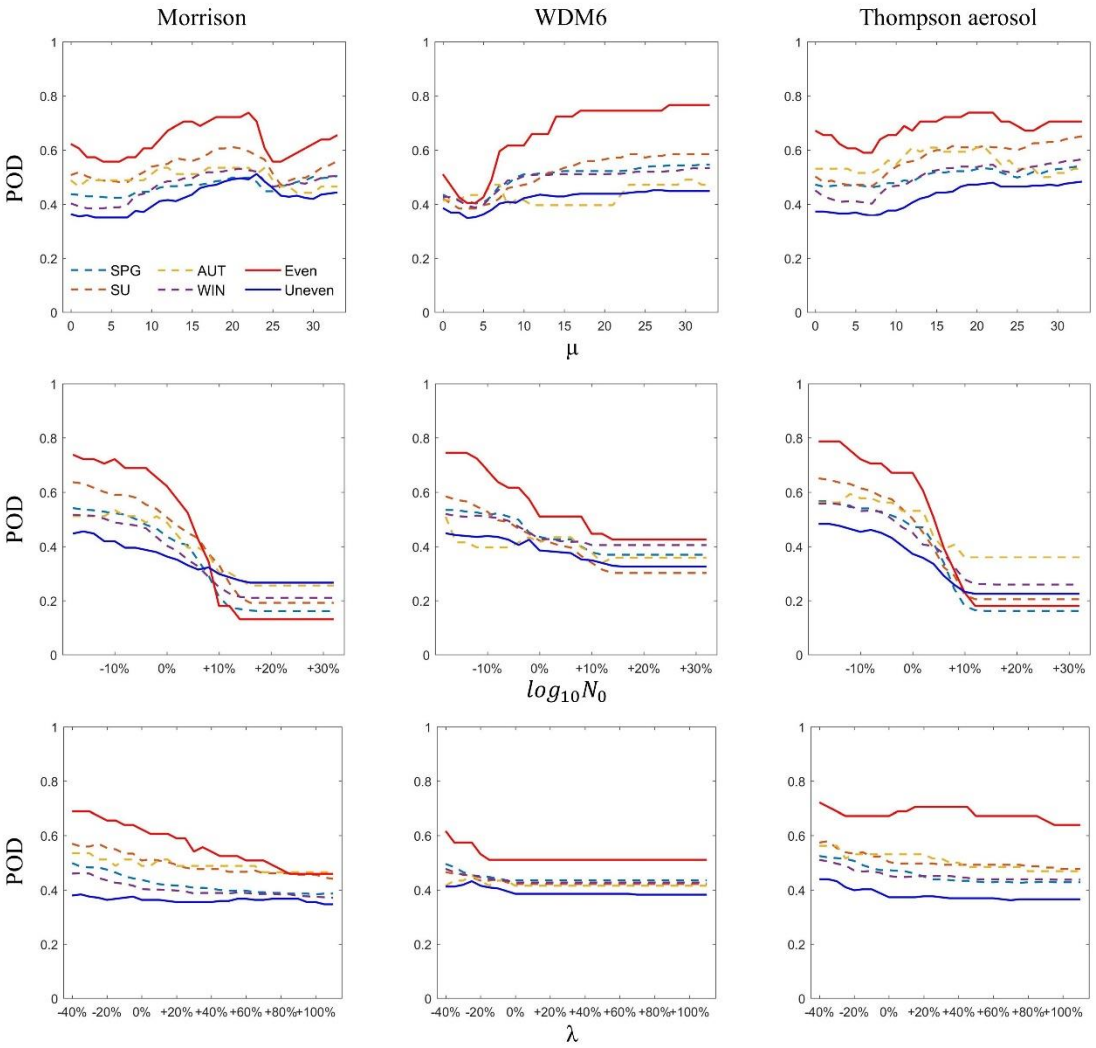

Figure 4. POD curves for a series of μ, $log_{10}N_0$, and λ values obtained from the WRF and disdrometer gamma DSD model for different types of rainfall events (scenarios A1–A4 as well as B1 and B2) and three microphysics schemes.

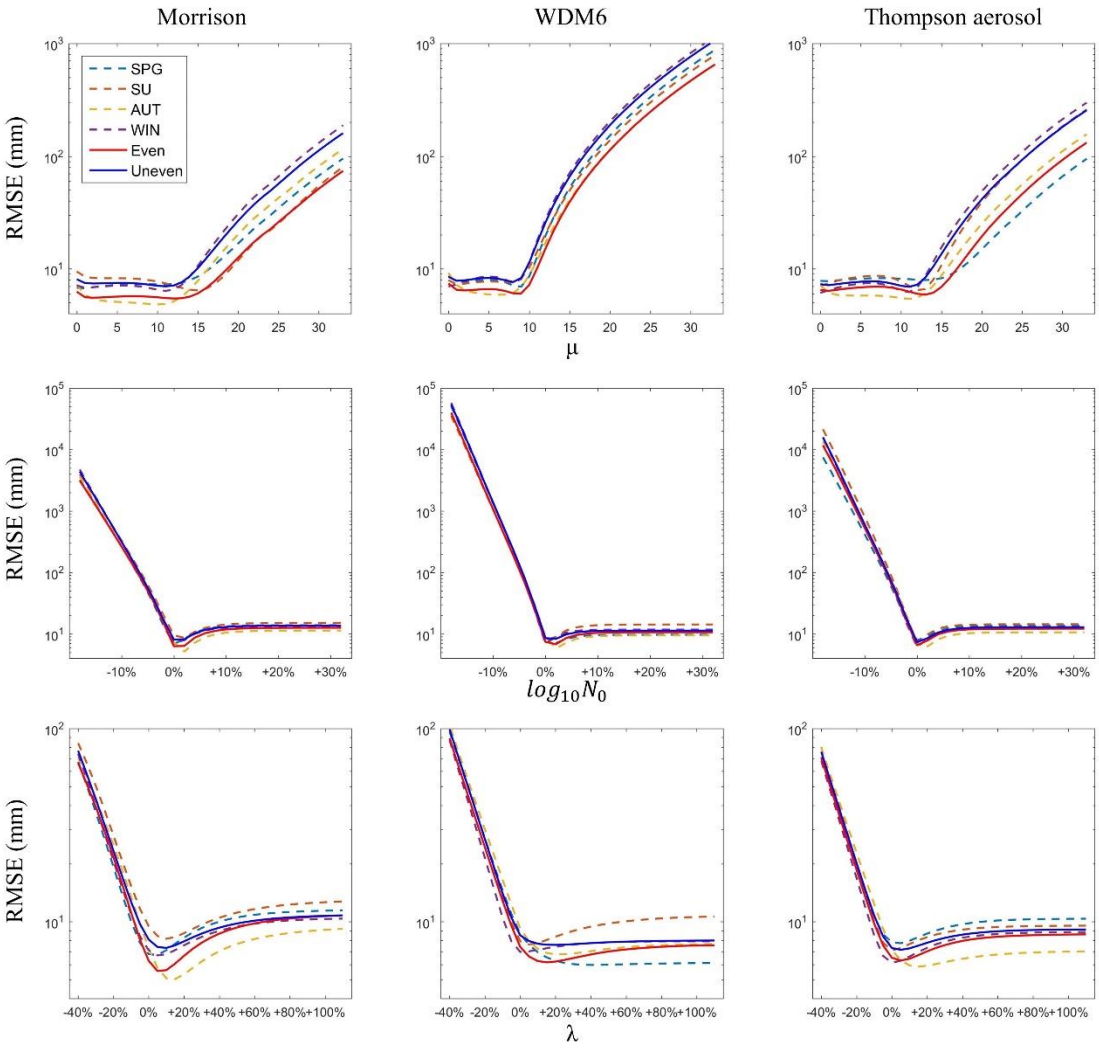

Figure 5. RMSE curves for a series of μ, $log_{10}N_0$, and λ values calculated from rainfall results of the WRF model and disdrometer for different types of rainfall events and three microphysics schemes.

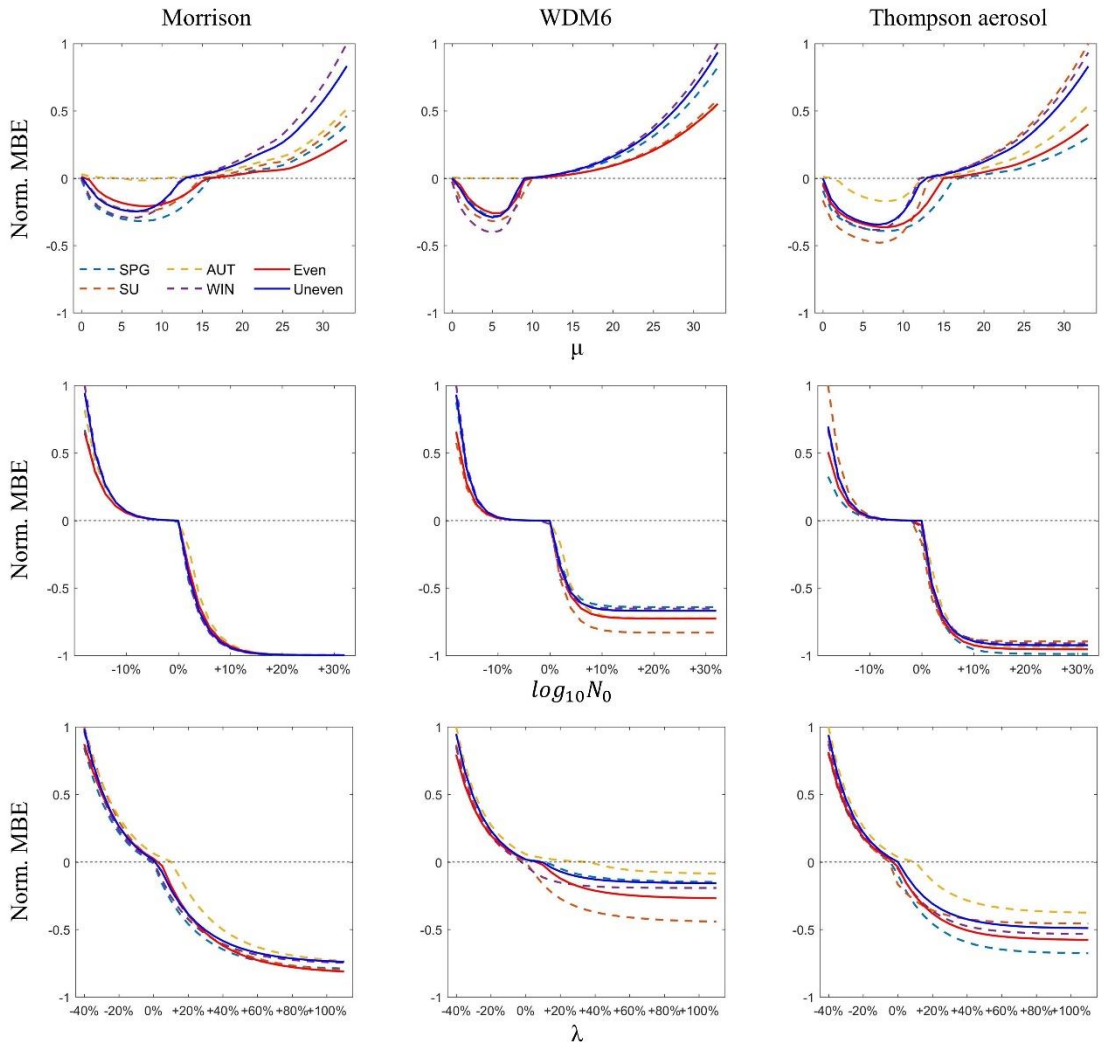

Figure 6. Normalized MBE for a series of μ, $log_{10}N_0$, and λ values of the WRF DSD model calculated from the WRF and disdrometer rainfall retrievals for different types of rainfall events and three microphysics schemes.

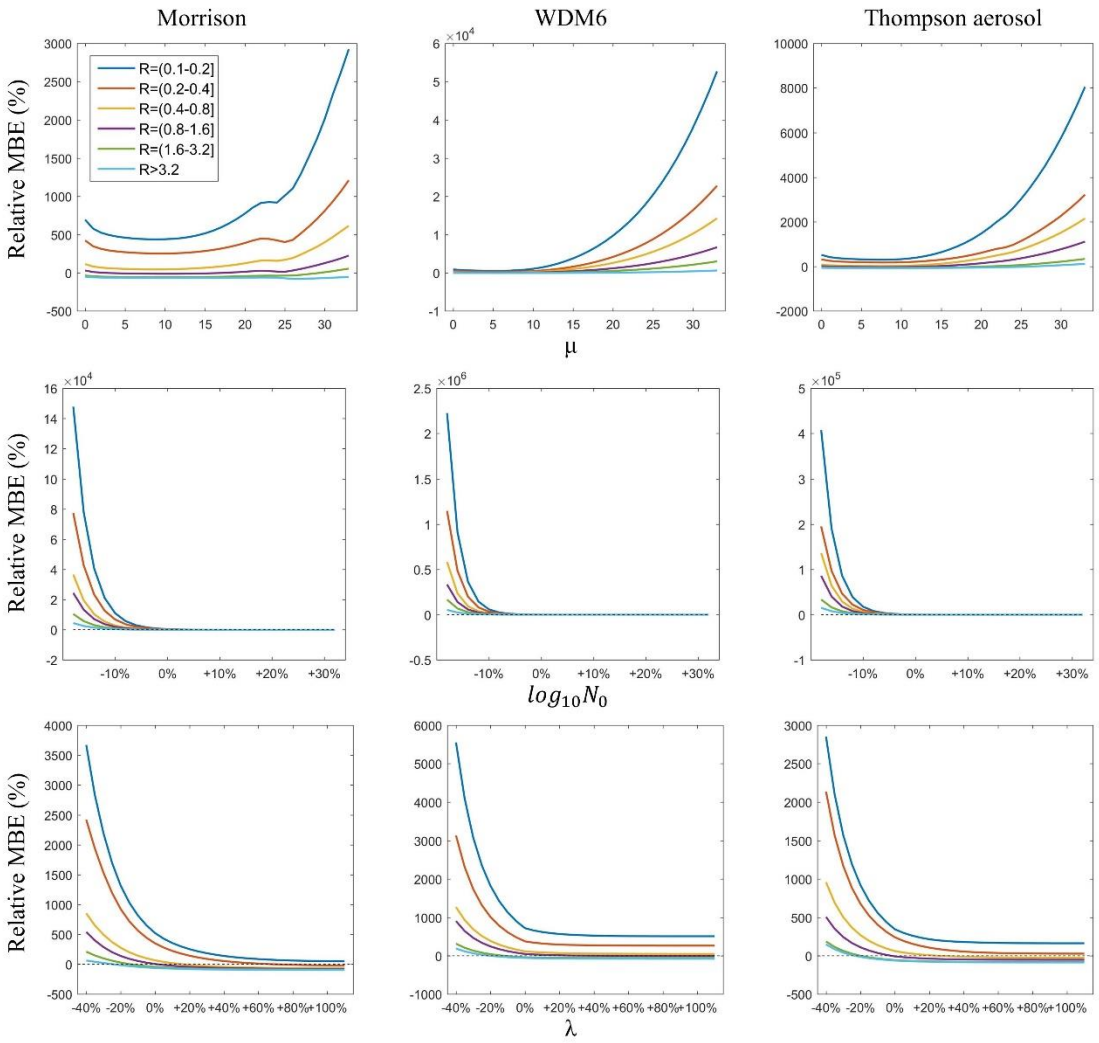

Figure 7. Relative biases for a series of μ, $log_{10}N_0$, and λ obtained from the WRF and disdrometer rainfall retrievals for different rainfall rates and microphysics schemes.

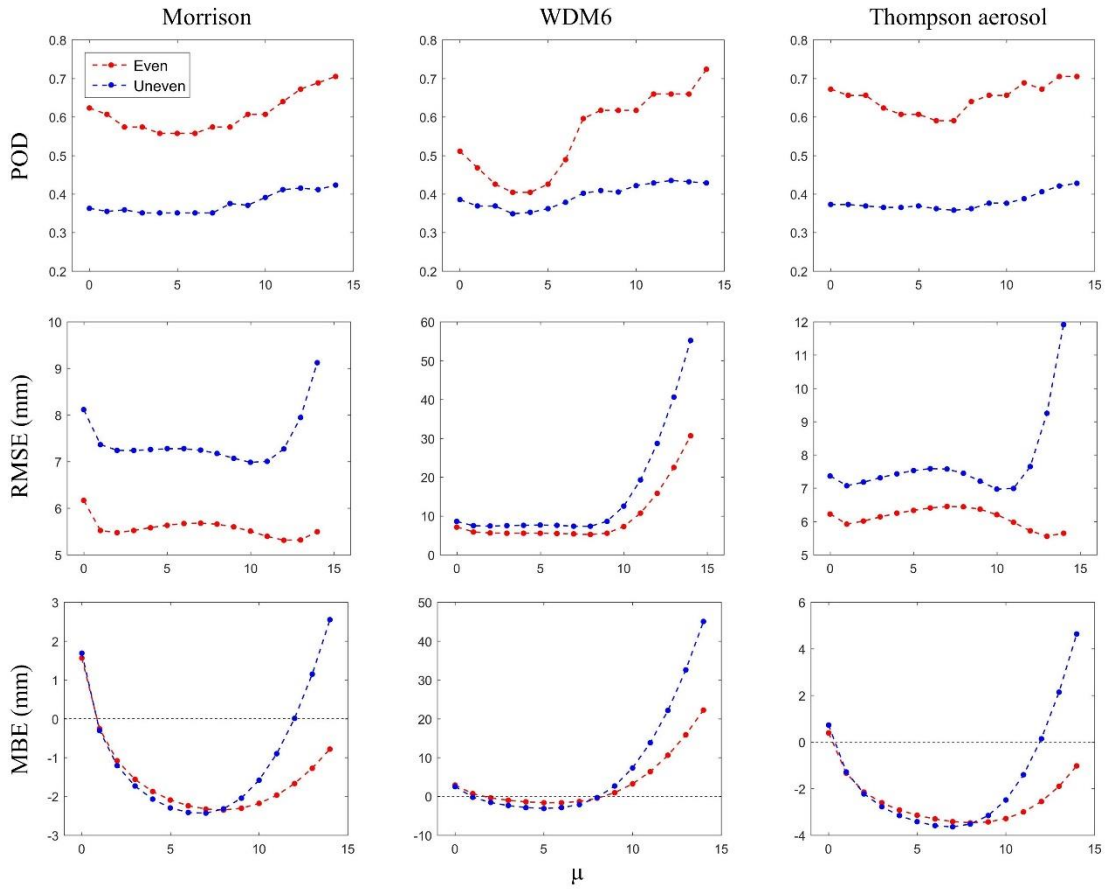

Figure 8. POD, RMSE, and MBE based on the gamma distribution of μ ranging from 0 to 14 for different microphysics schemes and rainfall types.

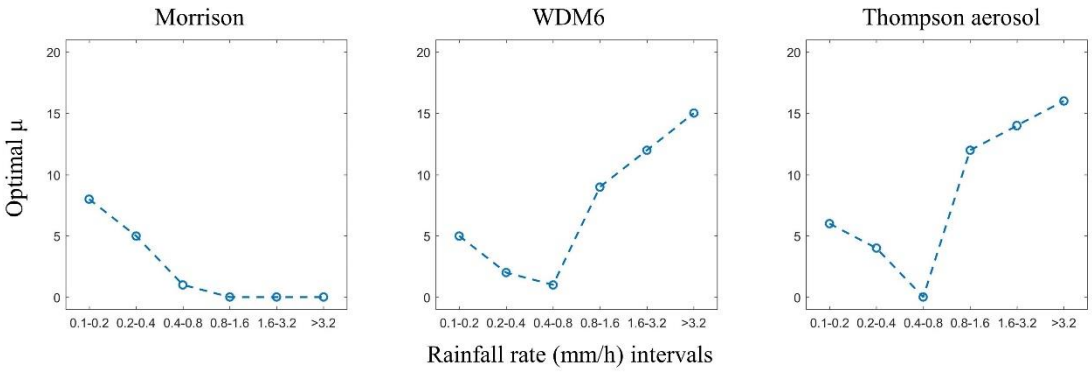

Figure 9. Optimal value of the shape parameter for different rainfall rate (mm/h) intervals of different microphysics schemes.

Table 1. Configurations of the WRF model for three nested domains.

Domain	Domain size (km)	Grid spacing (km)	Grid size	Time step (h)	Downscaling ratio
D01	360×360	18	21×21	3	-
D02	180×180	6	31×31	1	1:3
D03	60×60	2	31×31	0.25	1:3

Table 2. Floating ranges, intervals, and boundary conditions of shape, intercept, and slope parameters for the sensitivity analysis of WRF DSD parameterizations.

Parameters	Range	Interval	Lower limit	Upper limit
μ	0 - 33	1	/	/
$log_{10}N_0$	-18% - +31%	2%	1.3	5.5
λ	-40% - +110%	5%	1.0	11.7

Table 3. Physical range and median of DSD parameters $log_{10}N_0$ and λ of the disdrometer and three microphysics schemes of the WRF model.

DSD set	$log_{10}N_0$			λ		
	Min	Median	Max	Min	Median	Max
Disdrometer	1.3	3.9	5.5	1.0	4.6	11.7
Morrison	0.8	3.6	5.5	1.4	3.7	14.0
WDM6	1.0	5.3	6.7	1.3	7.8	19.8
Thompson aerosol	0.8	4.0	5.8	1.5	4.8	14.5

Table 4. Comparison of POD, RMSE (mm), and MBE (mm) among the three microphysics schemes for rainfall events in the four seasons (scenarios A1–A4) and with even and uneven rain (scenarios B1–B2). "TAA" represents the Thompson aerosol-aware scheme.

	POD			RMSE (mm)			MBE (mm)		
Scenarios	Morrison	WDM6	TAA	Morrison	WDM6	TAA	Morrison	WDM6	TAA
A1	0.45	0.44	0.50	7.06	7.42	7.78	0.78	0.89	-0.07
A2	0.47	0.35	0.55	8.47	8.18	7.12	-0.20	-2.46	-0.63
A3	0.55	0.33	0.47	8.04	6.87	7.24	4.78	2.32	3.10
A4	0.41	0.43	0.46	6.52	5.83	5.63	0.81	-1.11	-0.25
B1	0.62	0.47	0.67	6.16	5.88	6.23	1.56	0.67	0.39
B2	0.36	0.37	0.37	8.11	7.46	7.37	1.69	-0.24	0.72

Table 5. Comparison of relative bias (%) among the three microphysics schemes for different rainfall rates (scenarios C1–C6).

Scenarios	Morrison	WDM6	Thompson
C1	694.34	700.65	518.24
C2	423.280	382.04	315.92
C3	113.15	121.52	82.42
C4	29.54	35.85	10.56
C5	-36.47	-40.81	-42.75
C6	-51.76	-55.14	-56.22